Binder effect on ZnAl₂O₄-containing high-alumina refractory castables

V. S. Pinto[1], A. P. Luz[1,2]*, O.H. Borges[2], V. C. Pandolfelli[1,2]

[1] Federal University of São Carlos, Materials Engineering Department,

Rod. Washington Luiz, km 235, São Carlos–, SP, 13565-905, Brazil.

[2] Federal University of São Carlos, Graduate Program in Materials Science and Engineering, São Carlos–SP, Brazil.

*Corresponding author at: t*el.: +55-16-33518601

E-mail: anapaula.light@gmail.com or analuz@ufscar.br

Abstract

In situ spinel (MgAl₂O₄, ZnAl₂O₄, etc.) formation in alumina-based castables has been pointed out as a key issue in the refractory area, as it may enhance the mechanical properties and corrosion resistance of such materials. Nevertheless, the generation of these compounds is usually accompanied by a large volume expansion, which may induce crack formation in the resulting microstructure. Aiming to investigate the influence of zinc and magnesia spinel generation on the properties of alumina-based castables, three vibratable compositions, containing calcium aluminate cement or hydratable alumina as binders, were designed and characterized in this work. Different experimental tests were carried out to analyze the produced samples, such as: cold flexural strength, apparent porosity, hot elastic modulus, assisted sinterability, corrosion cup-tests, etc. According to the results, ZnAl₂O₄ was mainly formed above 800 °C, favoring an earlier sintering of the samples. The addition of high amounts of ZnO or MgO (3 wt% to 9.4 wt%) to the castables resulted in the expansion of the samples during their first thermal treatment up to 1500 °C, reaching dL/L₀ values equivalent to 1.16 % up to 2.35 %. Thermodynamic simulations indicated that spinel phase presented higher chemical stability when in contact with the evaluated synthetic slag at 1500 °C. Depending on the corrosion cup-test procedure (free or under constraint), different results of the slag infiltrated area were obtained (13.7 % to 20.5 %) and, the combination of two different spinel phases (MgAl₂O₄ and ZnAl₂O₄) in a castable composition resulted in a refractory with enhanced corrosion behavior when the tests were carried out under constraint.

Keywords: spinel, ZnO, refractory castable, binder, expansion

1. Introduction

Various efforts have been made in the refractory field to develop castable products with improved performance that could withstand the harsh operational conditions of industrial processes. Thus, not only the selection and combination of suitable raw materials, but also the processing methods and the microstructural changes during the first heating step of such materials are important aspects that should be carefully addressed.

The *in situ* generation of spinel phases (i.e., $MgAl_2O_4$, $ZnAl_2O_4$, etc.) in alumina-based castable compositions has been investigated by many researchers [1–10], as these compounds play an important role in increasing the mechanical behavior as well as the slag corrosion resistance of such ceramic systems. Regarding its crystalline structure, as reported by Bi et al. [11], the oxygen anions in AB_2O_4 spinel (where A and B are cations with valence 2+ and 3+, respectively) present face-centered-cubic (fcc) close packing. The unit cell contains 32 oxygen anions, 16 octahedral cations, and 8 tetrahedral cations in the normal spinel structure. A^{2+} cations occupy the tetrahedral vacancies and the B^{3+} cations are in the octahedral ones. However, in the inverse-spinel structure, the A^{2+} and one-half of the B^{3+} cations occupy the octahedral vacancies, and the remaining one-half of the B^{3+} cations are in the tetrahedral ones. Such a complex structure results in interesting features, as the spinel phase can trap Mn^{2+}, Fe^{2+} and Fe^{3+} ions in its structure via solid solutions. Consequently, spinel-containing refractories usually present enhanced corrosion resistance as the withdrawal of these ions from the slag may result in a silica-rich viscous liquid, which will not easily infiltrate into the ceramic lining porosity [12–14].

Most of the studies presented in the literature are focused on the investigation of $MgAl_2O_4$ formation and its role on alumina-based refractories performance [2,3,9,15–17]. Zinc aluminate spinel ($ZnAl_2O_4$) has received less attention, although it has a high melting temperature (1950

°C), regular thermal expansion coefficient (7×10^{-6} °C^{-1} in the 25 °C - 900 °C range) and good resistance to acids and alkali [6,18]. Additionally, theoretical studies carried out by Xu et al. [19,20] have reported the likelihood of tailoring some properties of $ZnAl_2O_4$-based ceramics by changing the stoichiometry of this phase, which may expand its application.

$ZnAl_2O_4$ formation takes place through the reaction between ZnO and Al_2O_3 generating *(i)* a solid solution of zinc oxide in aluminum oxide in the 600 °C to 700°C temperature range, followed by *(ii)* a disordered spinel structure between 700 °C and 800 °C, which will be converted into an ordered one at temperatures above 800 °C [6,21]. Therefore, such transformations may also favor an earlier sintering of the refractories, resulting in improved mechanical performance at intermediate temperatures (> 700 °C) [6]. Additionally, zinc oxide has the ability to speed up the formation of calcium aluminate phases (i.e., $CaAl_4O_7$, $CaAl_{12}O_{19}$, etc.) and $MgAl_2O_4$ (MA) in Al_2O_3-CaO-MgO containing compositions [22,23]. Wang et al. [22] pointed out that ZnO accelerated the formation of MA phase at high temperatures in Al_2O_3-MgO-$CaCO_3$ ceramics by replacing Mg^{2+} by Zn^{2+} in the spinel grains to give rise to a uniform $(Mg_{1-x}Zn_x)Al_2O_4$ solid solution. Besides that, ZnO addition affected the evolution of $CaAl_{12}O_{19}$ grains from plate-like to equiaxed structures, which favored an easier development of the MA grains and improved the densification of the prepared specimens [22].

However, the in situ generation of $ZnAl_2O_4$, $MgAl_2O_4$ and calcium aluminates in refractories is accompanied with a large volume expansion [24–26]. Li et al. [6] stated that zinc carbonate or hydroxide could be used as alternative materials to suppress volume expansion and improve the ceramics' volume stability, as the decomposition of such compounds during the specimens first heating would give rise to micropores in the refractory structure, providing space to counter-balance the expansion related to the formation of spinel and calcium aluminate compounds at high temperatures. Nevertheless, both recent investigations [6,8], considering the addition of $Zn(OH)_2$ and basic zinc carbonate in refractory castables, only analyzed the

incorporation of small contents of these additives (0 to 0.66 wt%) in high-alumina calcium aluminate cement-bonded castables.

Based on these aspects and knowing that previous studies [15,27] highlighted that the optimal spinel content to improve the slag resistance and wear mechanisms of Al_2O_3-MgO refractories would be in the 20 wt% - 25 wt% range, this work addressed the evaluation of alumina-based castables containing higher amounts of ZnO and/or MgO (3 wt% – 9.4 wt%) as precursor materials for spinel formation. Hydratable alumina and calcium aluminate cement were selected as binders and the samples' characterization were carried out to infer the influence of the phase transformations on the thermo-chemical-mechanical performance of such materials at high temperatures.

2. Experimental

2.1 – Evaluated compositions

Three vibratable castables (Table 1) were designed considering the Alfred's particle packing model and distribution coefficient (q) equal to 0.26 [28]. A fixed amount of binder (6 wt%) and the equivalent content of zinc oxide or a mixture of zinc and magnesium oxides were selected to give rise to a total of approximately 21 wt% of spinel phases ($MgAl_2O_4$ and/or $ZnAl_2O_4$), after firing these refractories at high temperatures.

Table 1 – General aspects of the designed castables evaluated in this work.

Raw materials (wt. %)	AZA	AZC	AZMA
Tabular alumina (d < 6 mm)	79.6	79.6	81.3
Calcined alumina (CL370)	3	2	3
Reactive alumina (CT3000SG)	2	3	2
Magnesia (d < 212 μm)	-	-	3
Zinc oxide (d < 20 μm)	9.4	9.4	4.7

Calcium aluminate cement (Secar 71)	-	6	-
Hydratable alumina (Alphabond 300)	6	-	6

Tabular alumina (aggregates, d < 6 mm, Almatis, Germany), reactive and calcined aluminas (CL370 and CT3000SG, Almatis, Germany), magnesium oxide (dead-burnt, M30-B, d < 212 μm, RHI-Magnesita, Brazil) and zinc oxide (analytical reagent grade, d < 20 μm, LabSynth, Brazil) were selected as raw materials. The addition of hydratable alumina (HA, Alphabond 300, Almatis, Germany) to AZA and AZMA (Table 1) as binder was analyzed, as the former composition would favor only the $ZnAl_2O_4$ formation during the samples' thermal treatments, whereas the latter would induce the generation of $ZnAl_2O_4$, $MgAl_2O_4$ or even a complex spinel structure, $(Mg_{1-x}Zn_x)Al_2O_4$. A third castable (AZC) was also evaluated, but in this case calcium aluminate cement (CAC, Secar 71, Imerys Aluminates, France) was incorporated as binder into the mixture. Thus, AZC should present $ZnAl_2O_4$ and calcium aluminates in its microstructure after firing.

2.2 – Processing steps and characterization of the prepared samples

The preparation of the designed compositions consisted of initially adding 0.2 wt% of a polyethylene glycol-based dispersant (Castament FS 60, Basf, Germany) to the dry-powders and then a dry and wet homogenization steps were carried out in a home-made rheometer device [29] with further incorporation of distilled water to the materials. The water demand for each tested composition was adjusted (to be presented in Table 5) to obtain vibratable flow values (ASTM C 1445) around 150 %. The molded samples were cured at 30 °C for 24 h and dried at 110 °C for another 24 h. The setting behavior of the prepared castables was also analyzed via ultrasonic measurements at room temperature (~ 23 °C) for 24 h, using the UltraTest device, IP-8 measuring system (Germany).

Permanent dimensional change (PLC, ASTM C113-14) of bar samples (150 mm x 25 mm x 25 mm) was carried out based on measurements of the specimens' length before and after firing at 800 °C, 1000 °C, 1200 °C and 1500 °C for 5 h. A total of 5 specimens were analyzed for each selected condition to identify the influence of the expected phase transformations on the castables' final dimension. Additionally, the linear dimensional change (assisted sinterability – AS) and thermal stability (refractoriness under load - RUL) of the castables were monitored *in situ* up to 1500 °C. For this purpose, cylindrical specimens (height and external diameter = 50 mm and central inner diameter = 12.5 mm) were prepared according to 51053 DIN standard and calcined at 600 °C for 5 h (AS) or pre-fired at 1500 °C for 5 h (RUL). The calcined samples were submitted to a heating rate of 3 °C/min up to 1500 °C and kept under a compressive load of 0.02 MPa for the AS measurements. For the RUL tests, the castables fired up to 1500 °C for 5 h were analyzed under a compressive load of 0.2 MPa and a heating rate of 5 °C/min.

The influence of the phase transformations on the castables' elastic modulus (E) behavior was analyzed according to the ASTM C 1198-91 standard using the bar resonance technique (Scaneastic equipment, ATCP, Brazil), which is based on the sample excitation and detection of the correspondent vibration spectrum, via piezoelectric transducers [30]. Tests were carried out in the 30 °C - 1400 °C temperature range with heating and cooling rates of 2 °C/min. Aiming to identify the likely phases developed in the microstructure of the designed castables and their influence on the obtained E profiles, simplified mixtures based on more reactive components (d < 200 μm, Table 2), better representing the matrix of the refractory castables, were prepared and evaluated via X-ray diffraction measurements and thermodynamic calculations (with the help of FactSage software, version 6.4, developers CRCT (Canada) and GTT (Germany)). Firstly, the dry powders were mixed with distilled water (20 wt%) for approximately 5 min at room temperature. The obtained suspensions were molded as cylindrical samples (30 mm x 30

mm) and kept at 30 °C for 24 h. After that, a drying step was conducted at 110 °C for another 24 h and the specimens were fired at 1000 °C, 1200 °C or 1500 °C for 5 h.

X-ray diffraction tests of the ground samples were carried out using D8 Focus equipment (Bruker, Karlsruhe, Germany) and with CuKα radiation [λ = 1.5418 Å], nickel filter, 40 mA, 40 mV, 2θ = 4° - 80° and scanning step = 0.02°. Rietveld simulations were also performed using the Topas software (version 4.2, Bruker, Germany) to estimate the amount of each phase contained in the fired samples, ensuring Goodness of Fit (GOF) < 1.02 and weighted profile R-factor (RWP) < 1.3 %.

Table 2 – Matrix (d < 200 μm) components of the castable's compositions.

Raw materials (wt. %)	AZA	AZC	AZMA
Tabular alumina (d < 200 μm)	44.9	44.9	49.5
Calcined alumina (CL370)	8.1	5.4	8.1
Reactive alumina (CT3000SG)	5.4	8.1	5.4
Calcium aluminate cement (Secar 71)	-	16.2	-
Magnesia (d < 212 μm)	-	-	8.1
Hydratable alumina (Alphabond 300)	16.2	-	16.2
Zinc oxide (d < 20 μm)	25.4	25.4	12.7

Corrosion cup tests were conducted with cylindrical samples (with an external d = 50 mm, h = 50 mm and a central inner role with 20 mm in diameter and 25 mm deep), which were divided into two groups (calcined and pre-fired ones, as they were heated up to 600 °C and 1500 °C for 5 h, respectively) and subjected to two distinct corrosion procedures (samples were free to expand or kept under constraint), as pointed out in Table 3. A total of 3 samples were analyzed for each studied condition and the chemical composition of the selected slag is shown in Table 4.

Table 3 – Corrosion procedures for the evaluation of the refractory castables.

Thermal treatment of the castables' before the corrosion tests	Free samples	Samples under constraint
600 °C for 5 h	The inner cup of the castables were filled in with 8 g of synthetic slag and the set (refractory + slag powder) was placed in an electrical furnace and heated up to 1500 °C for 2 h under a heating rate of 2 °C / min.	After their initial thermal treatment (600 °C or 1500 °C), 3 cylindrical samples of each composition were placed in a polymeric mold with the following dimensions: 230 mm x 114 mm x 64 mm. An alumina based castable (containing 6 wt% of hydratable alumina as binder) was prepared and cast around the cylinders. After curing (30 °C for 24 h) and drying (110 °C for 5 h) steps, the obtained blocks (containing the castables' cylinders in its structure) were also calcined at 600 °C for 5 h before placing the slag powder in the inner cup of the AZA, AZC and AZMA refractory samples. The corrosion experiments were carried out at 1500 °C for 2 h under a heating rate of 2 °C / min in an electric furnace.
1500 °C for 5 h		

Table 4 – Chemical composition of the selected synthetic slag.

Oxides (wt%)	SiO_2	TiO_2	Al_2O_3	Fe_2O_3	CaO	MgO	K_2O	SO_3	F
Slag	28.8	0.6	10.7	1.2	42.7	7.2	0.6	1.6	6.2

After cooling, the corroded samples (free or under constraint) were cut and had their cross sections observed using the Image J 1.42q software (Wayne Rasband, National Institutes of Health, USA) for the determination of the relative infiltrated area of the castable, as described in [31]. Additionally, thermodynamic calculations were carried out to predict the phases that should be formed during the initial slag-castable interaction, in the equilibrium condition at 1500 °C, using the FactSage software (version 6.4, databases = FactPS and FToxid, and the Equilib calculation modulus).

3. Results and Discussion

3.1 – Flowability and curing behavior

Table 5 shows the water demand and flowability values obtained for the designed castables after their processing step. The hydratable alumina (HA)-containing compositions (AZA and AZMA) required higher liquid content (4.6 wt% - 4.8 wt%) when compared with the cement (CAC)-bonded material (AZC), which is explained by the high specific surface area (around 150-200 m^2/g [32]) and reactivity of the former binder. Nevertheless, all castables presented similar vibratable flow values (in the range of 151 % to 158 %), providing a suitable casting of the samples.

Table 5 - Water demand and vibratable flow obtained for the evaluated castables.

Compositions	Water content (wt%)	Vibratable flow (%)
AZA	4.6	151
AZC	4.0	153
AZMA	4.8	158

The binders' action affected the setting and curing behavior of the samples, as pointed out in Fig. 1. The ultrasonic measurements were carried out at room temperature (~ 23 °C) and, initially, the HA-based materials presented faster setting, as depicted by the more significant increase of the ultrasonic wave propagation velocity detected after approximately 2 hours. However, AZA and AZMA also showed a further drop of the measured velocity (in the 5.5 to 8 h range), which might be related to the shrinkage of the samples (resulting in a slightly detachment of the sensors) or the generation of flaws (i.e., microcracks, voids, etc.) in the refractory microstructure, mainly for the MgO-containing composition due to $Mg(OH)_2$ formation. With the advance of curing time, the final velocity values obtained for AZA and AZMA were half of the one collected for the CAC-containing castable (AZC, Fig. 1).

Therefore, although the cement-bonded composition presented a slower setting (velocity increase around 4 h - 8 h) in the evaluated conditions, the greater ultrasonic velocity values obtained after 24 h of curing indicate that such material should present better green mechanical strength levels. The distinct performance of the HA and CAC-bonded materials is directly related to the binders' reaction mechanisms and the hydrated phases (crystalline or gel-like compounds) formed in such materials. More details of such transformations can be found in [33,34].
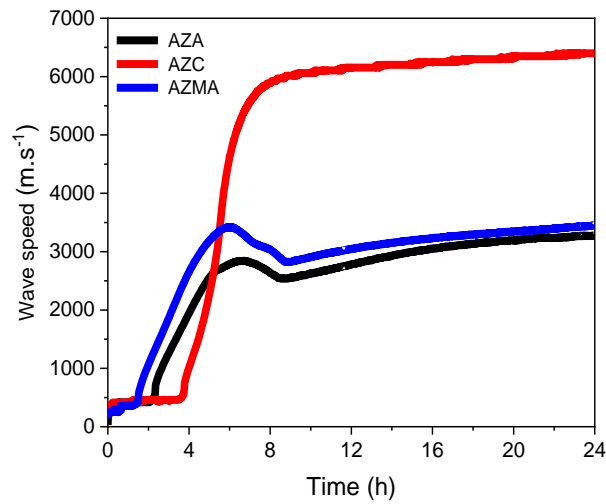
Figure 1 – Curing behavior of the castables as a function of time at room temperature (~ 23 °C).

3.2 – Samples' properties as a function of the temperature

Aiming to identify the effects associated with the in situ generation of $ZnAl_2O_4$, $MgAl_2O_4$ and calcium aluminates in the evaluated refractories, the castables' dimensional stability was analyzed after firing and cooling bar samples at different temperatures (permanent linear change, Fig. 2a) or following their expansion via the assisted sinterability technique (Fig. 2b and 2c).
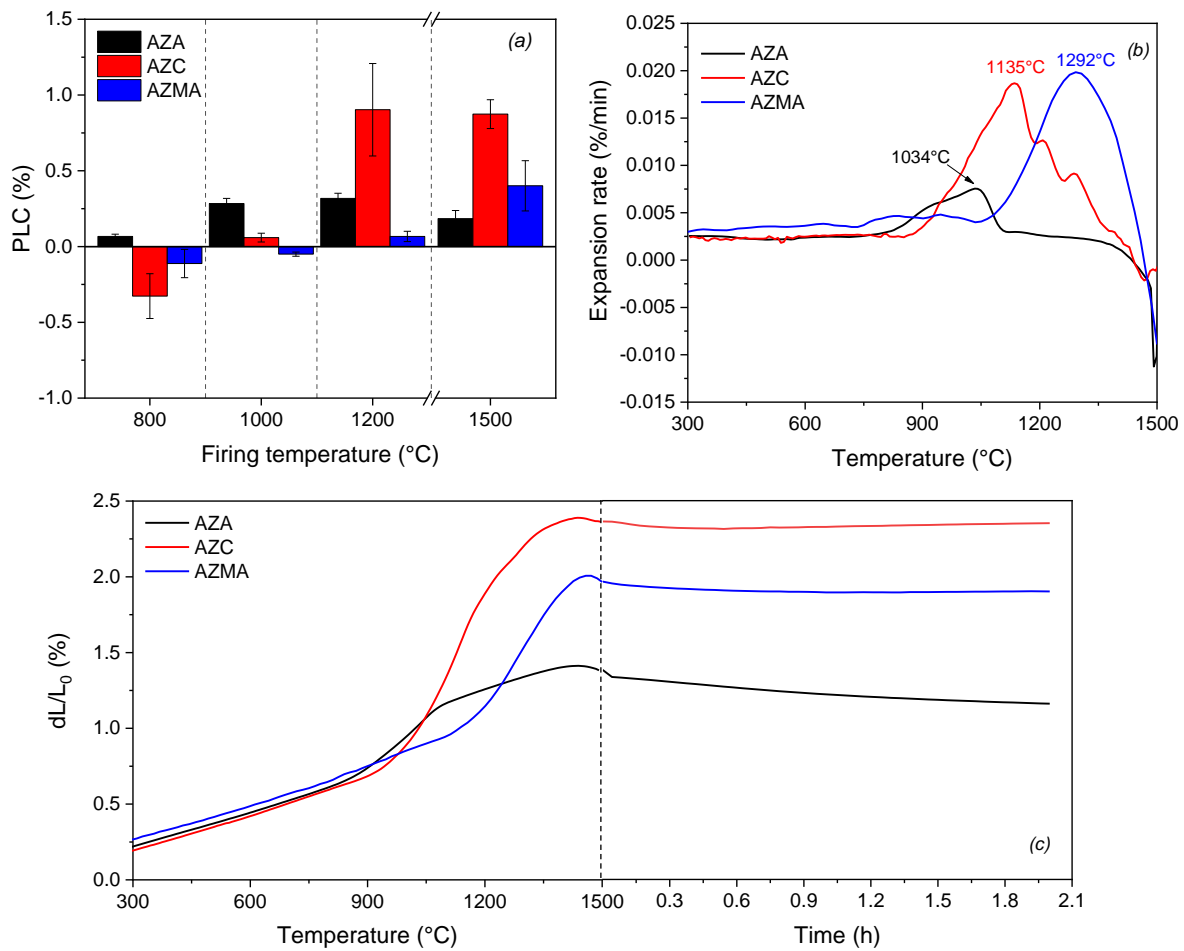
Figure 2 – (a) PLC and (b, c) *in situ* linear expansion of the castables as a function of the temperature.

Fig. 2a indicates that AZA samples expanded after thermal treatments at 800 °C, 1000 °C and 1200 °C for 5 h, reaching values ranging from 0.06 % up to 0.32 %. Nevertheless, when heating the same composition at higher temperature (1500 °C), a small decrease of the measured expansion was observed (0.18 %), which can be explained by the sintering and densification of the microstructure under such a condition. Despite using the same binding system, AZMA refractory showed shrinkage of the pieces when firing them at lower temperatures (800 °C and 1000 °C, Fig. 2a) and an increase in their linear dimension could be detected only above 1200

°C. Shrinkage of around 0.32 % was identified for the AZC samples fired at 800 °C, whereas a more significant expansion (0.90 % and 0.87 %) could be detected mainly at high temperatures (1200 °C and 1500 °C, respectively).

The same trend identified in the permanent linear change measurements carried out at 1500 °C (final measured expansion = AZC > AZMA > AZA) was also seen via the sinterability technique (AS). Fig. 2b (first derivative of the dL/L_0 profiles shown in 2c) highlights the earlier expansion (around 800 °C - 900 °C) of AZA and AZC compositions, whereas AZMA samples presented a significant change in their dimensions mainly above 1100°C. The expansion rate peaks for each evaluated castable were identified at 1034°C (AZA), 1135°C (AZC) and 1292°C (AZMA). Besides that, Fig. 2c points out that, in all studied cases, the maximum dL/L_0 values were reached close to 1400 °C - 1430 °C. After that, a small but continuous decrease of the sample's dimension was detected up to the end of the test, resulting in final results equivalent to 1.16 %, 1.90 % and 2.35 % for AZA, AZMA and AZC, respectively (Fig. 2c). According to Braulio *et al.* [35,36], high alumina castables containing 6 wt% of MgO (with *in situ* formation of approximately 21 wt% of $MgAl_2O_4$) may present a maximum expansion level of 1.95 % (binder-free refractory, as magnesia was responsible for reacting with water and generating $Mg(OH)_2$ phase during curing step) for the AS tests, whereas the addition of 6 wt% of CAC to the same composition resulted in dL/L_0 close to 3 % at 1500 °C and under the same conditions as the ones analyzed in the present work. Thus, although high expansion values were obtained for the ZnO-containing refractories, these results are in tune with the data presented in the literature for other systems [35,36].

This behavior is related to the phase transformations that can take place in the refractories' microstructure during their first thermal treatment. Table 6 shows the estimated amount of the crystalline compounds contained in the matrix fraction (Table 2) of the evaluated materials, when analyzing simplified compositions (more reactive components of the castables, with

particle size < 200 μm) after firing at 1000 °C, 1200 °C and 1500 °C for 5 h. X-ray diffraction measurements and Rietveld calculations were carried out for each analyzed sample, resulting in the data presented below.

Table 6 – Estimated amount of the phases (wt%, obtained via Rietveld calculations) generated in the matrix composition of the designed castables.

Rietveld Calculations									
Compositions	Temperature (°C)	α-Al_2O_3	$Na_2Al_{22}O_{34}$	ZnO	$ZnAl_2O_4$	$CaAl_4O_7$	$CaAl_{12}O_{19}$	MgO	$MgAl_2O_4$
AZA	1000	55.1	1.8	1.2	41.9	-	-	-	-
	1200	32.4	1.2	-	66.3	-	-	-	-
	1500	32.4	-	-	67.6	-	-	-	-
AZC	1000	60.5	1.9	8.9	28.6	-	-	-	-
	1200	21.2	-	-	65.8	13.1	-	-	-
	1500	2.2	-	-	66.8	17.4	13.6	-	-
AZMA	1000	53.6	2.0	0.3	32.4	-	-	11.7	-
	1200	50.6	1.6	-	34.9	-	-	7.9	4.9
	1500	34.8	-	-	37.9	-	-	-	27.4

XRD JCPDS files: α-Al_2O_3 = 81-1667; $Na_2Al_{22}O_{34}$ = 31-7263; ZnO = 79-206; $ZnAl_2O_4$ = 74-1136; $CaAl_4O_7$ = 76-706; $CaAl_{12}O_{19}$ = 84-1613; MgO = 87-651; $MgAl_2O_4$ = 75-1798.

Corundum (α-alumina), $Na_2Al_{22}O_{34}$ (β-alumina), ZnO and $ZnAl_2O_4$ spinel (generated in situ) could be identified in all evaluated compositions after firing at 1000 °C (Table 6). Moreover, periclase (MgO) was still detected in AZMA samples at this temperature, pointing out the need of higher thermal energy levels to induce $MgAl_2O_4$ formation in the selected time frame (5 hours) applied during the thermal treatments. The calculated Gibbs free energy for $ZnAl_2O_4$ and $MgAl_2O_4$ formation (Eq. 1 and 2) confirms the greater likelihood of the former reaction product to be found in the designed compositions at 1000 and 1200°C, whereas magnesium aluminate spinel generation becomes more favorable when increasing the temperature (Table 7). Although, Eq. 2 leads to negative ΔG values, $MgAl_2O_4$ formation still depends on the interaction of the initial raw materials and the kinetic aspects associated with

this transformation. Hence, the lack of this phase in AZMA samples fired at 1000 °C indicates that the thermodynamic equilibrium was not achieved in the experimental tests.

$$ZnO + Al_2O_4 \rightarrow ZnAl_2O_4 \tag{1}$$
$$MgO + Al_2O_4 \rightarrow MgAl_2O_4 \tag{2}$$

Table 7 – Calculated Gibbs free energy for the spinel phases formation at high temperatures.

Compounds	ΔG (kJ/mol)		
	1000 °C	1200 °C	1500 °C
$ZnAl_2O_4$	-36.61	-35.30	-33.33
$MgAl_2O_4$	-31.49	-32.98	-35.43

All ZnO was consumed for $ZnAl_2O_4$ formation when firing the samples at 1200 °C (Table 6). Besides that, $CaAl_4O_7$ (CA_2) and $MgAl_2O_4$ was generated in AZC and AZMA compositions, respectively. The expansive features of these phases' formation justify the significant increase of the samples' linear dimension in such conditions, as pointed out in Fig. 2. However, unreacted MgO was still present in AZMA, indicating that a complete $MgAl_2O_4$ formation was not accomplished at 1200 °C.

Raising the firing temperature from 1200 °C to 1500 °C did not result in significant changes in AZA phase composition (Table 6). On the other hand, corundum consumption was identified for AZC, giving rise to $CaAl_4O_7$ (CA_2) and $CaAl_{12}O_{19}$ (CA_6). In this case, alumina is the limiting reagent in the matrix fraction and, when considering the overall refractory composition (comprised by aggregates and fine components), it is expected that the remaining CA_2 phase should also react with the coarse tabular alumina particles to generate mainly CA_6 at 1500 °C. Hence, the high content of $ZnAl_2O_4$ and calcium aluminates (CA_2 and/or CA_6) phases is responsible for the greater expansion of AZC castable (Fig. 2). AZMA only presented corundum, $ZnAl_2O_4$ and $MgAl_2O_4$ phases in its composition at 1500 °C, where the sum of the

spinel contents (65.3 %) was similar to the one of $ZnAl_2O_4$ found in AZA and AZC (67.6 % and 66.8 %, respectively). Although $ZnAl_2O_4$ and $MgAl_2O_4$ were evaluated with the Rietveld analyses as separated compounds, they actually could be found as a $[(Mg_{1-x}Zn_x)Al_2O_4]$ solid solution. Nevertheless, the present study did not identify any peak position displacement (which could indicate at first the formation of this complex spinel) and further investigation is required.

When comparing the amount of the estimated phases contained in the castables' matrix samples (Table 6) with the results predicted by the thermodynamic calculations (Table 7), some differences in the obtained values could be observed, which is related to the fact that the latter represents a thermochemical equilibrium condition without taking into consideration the physical aspects of the raw materials (their particle size, scattering in the resulting microstructure, etc.) and kinetic ones, that influence the reactions rate at the selected temperatures. No unreacted ZnO and MgO are expected to be found at 1000°C and 1200°C, when firing AZA and AZMA compositions, as indicated in Table 7. Besides that, all alumina should be consumed for the formation of CA_2, CA_6 and spinel(ss) in AZC in the 1000-1500°C range. Although CA_6 generation is predicted to take place at 1000°C, the X-ray diffraction results indicated that such a phase is only formed at higher temperatures (Table 6).

The total amount of predicted spinel phase (which is a non-stoichiometric one) varies around 57.22 to 63.90 wt.% in the evaluated temperatures (Table 8). On the other hand, the experimental results, shown in Table 6, pointed out slightly higher contents for this phase at 1500°C (from 65.8 to 67.6%) and a reduced amount of this compound when the samples were fired mainly at 1000°C. Thus, the evaluated castables did not reach the equilibrium as predicted by FactSage and, to achieve this condition, the prepared samples should be kept at higher temperatures for longer times to allow all phase transformations to be completed.

Table 8 – Predicted phases (wt%, obtained via thermodynamic simulations) generated in the matrix composition of the designed castables.

Compositions	Temperature (°C)	α-Al_2O_3	$NaAl_{19}O_{14}$[*]	$CaAl_4O_7$	$CaAl_{12}O_{19}$	Spinel (ss)	Estimated amount of each main phase contained in spinel(ss) (%)	
							$ZnAl_2O_4$	$MgAl_2O_4$
AZA	1000	40.80	1.58	-	-	57.62	100	-
	1200	40.05	1.58	-	-	58.37	100	-
	1500	36.57	1.58	-	-	61.88	100	-
AZC	1000	-	1.26	10.61	30.62	57.50	100	-
	1200	-	1.26	10.97	29.71	58.06	100	-
	1500	-	1.26	12.55	25.64	60.54	100	-
AZMA	1000	41.17	1.58	-	-	57.22	62.35	37.65
	1200	40.76	1.58	-	-	57.66	62.47	37.53
	1500	34.52	1.58	-	-	63.90	61.47	38.53

*Although different than the β-alumina detected in the experimental results (Table 6), $NaAl_{19}O_{14}$ is the only equivalent phase available in FactPS and FToxid databases.

Aiming to investigate the influence of the mentioned transformations on the thermomechanical performance of the castables, in situ hot elastic modulus measurements were also carried out from room temperature up to 1400 °C. Fig. 3 shows the elastic modulus (E) profiles of the dried samples.
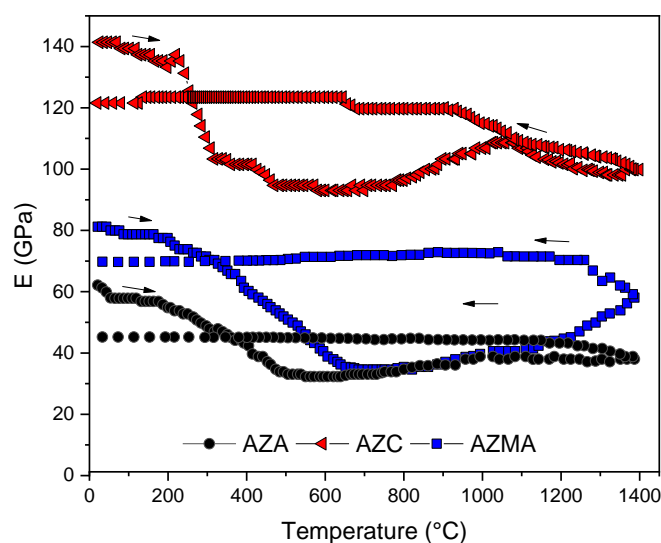
Figure 3 – *In situ* hot elastic modulus of the designed castables containing ZnO (AZA, AZC and AZMA) and a reference composition containing 94 wt% of alumina and 6 wt% of MgO (AM). Samples were cured at 30 °C for 24 h and dried at 110 °C for another 24 h before testing.

AZC showed the highest initial elastic modulus (142 GPa, Fig. 3) compared to the HA-bonded (AZA and AZMA) castables, indicating the enhanced performance of calcium aluminate cement in providing higher green mechanical strength development after curing and drying steps. Knowing that all compositions comprised hydraulic binders, heating the refractories above 110 °C led to the decomposition of the generated hydrates (i.e., aluminum hydroxides, magnesium hydroxide, etc., [33,34]). Consequently, all E profiles presented a decay of the measured values mainly in the 200 °C - 600 °C temperature range. The beginning of the sintering process (with the increase of the samples' stiffness) could be identified above 800 °C for ZnO-containing (AZA, AZC and AZMA) samples, attesting that $ZnAl_2O_4$ formation induced an earlier improvement of the thermomechanical performance of such materials, as pointed out in the literature [22]. After reaching the maximum tested temperature (1400 °C), few changes in the castables' elastic modulus were observed during the cooling step, and the

following sequence was obtained regarding the E values after the thermal treatment: 121 GPa (AZC) > 70 GPa (AZMA) > 48 GPa (AZA). No thermal expansion mismatch between the generated phases, indicated by a drop in the E values during cooling, was detected.

Based on the E results at 1400 °C (Fig. 3), it was expected that ZnO-containing samples should not present a great deformation at high temperatures due to the limited liquid phase formation predicted for such systems. This performance was attested after subjecting the prepared compositions to refractoriness under load (RUL) measurements (results not shown here), as only expansion and no deformation was detected for the designed refractories up to 1500°C.

Fig. 4 shows the cold flexural strength and apparent porosity of AZA, AZC, AZMA castables after their drying and firing at different temperatures. The CAC-bonded samples presented higher cold mechanical resistance in all evaluated conditions, which is explained by the action of the cement in the development of a more efficient binding effect than hydratable alumina. Although the decomposition of the CAC-based hydrates tends to increase the porosity level of AZC samples when subjecting them to high thermal treatments (> 110 °C, Fig. 4b), the $ZnAl_2O_4$ and calcium aluminate generation (Table 6) in the microstructure enhances the flexural strength of this material (Fig. 4a). In general, AZA and AZMA refractories presented higher porosity, which can be related to the higher water demand of these materials during their processing steps, Table 5, as well as the formation and further decomposition of the gel-like hydrated phases derived from the hydration of HA [33,34]. Moreover, the increase of the flexural strength of the HA-bonded castables was mainly observed above 1000 °C, due to spinel ($ZnAl_2O_4$ and $MgAl_2O_4$) formation.
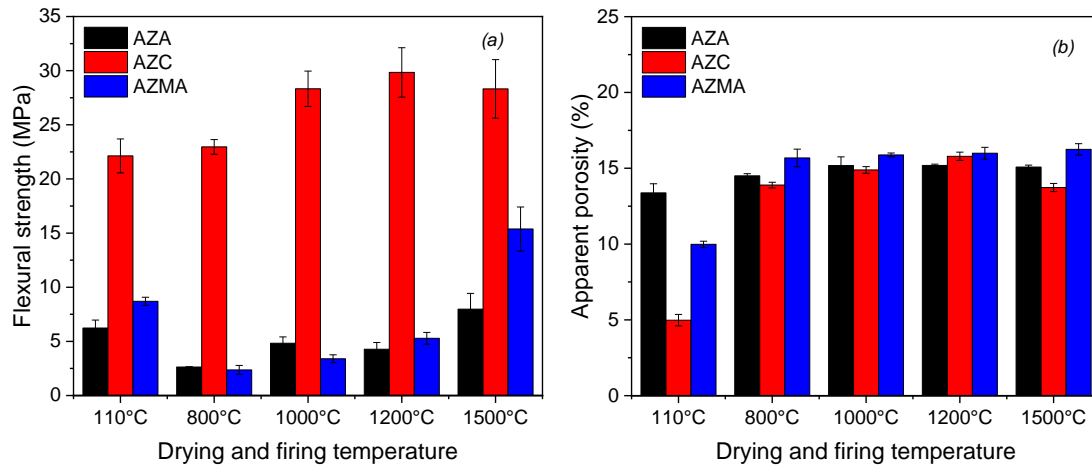
Figure 4 – (a) Cold flexural strength and (b) apparent porosity of the dried and fired castable samples.

MgO addition to AZMA tends to induce $Mg(OH)_2$ formation during the castable's processing steps, which might also explain the higher water demand (Table 5) for the preparation of this refractory. While heating such material, magnesium hydroxide will decompose (up to 400 °C [30]), releasing water vapour and leading to an increase in the overall porosity level (Fig. 4b). Consequently, at higher temperatures (> 800 °C), the formed $ZnAl_2O_4$ and $MgAl_2O_4$ phases should be accommodated in the resulting microstructure, which will influence the overall expansion and enhance thermomechanical behavior.

3.3 Corrosion and thermodynamic simulations

Aiming to analyze the influence of the in situ spinel formation on the corrosion resistance of the castables, cup-tests were carried out at 1500 °C for the calcined (660 °C for 5 h) and pre-fired (1500 °C for 5 h) samples. Additionally, two different conditions were tested: (i) the

samples were kept free (as usual) during the corrosion measurements or (ii) under constraint, with limited freedom to expand during the heating process and when in contact with the molten slag (see Section 2 for further details). Fig. 5 indicates the calculated slag infiltrated area after measuring the samples' region where liquid penetration took place.
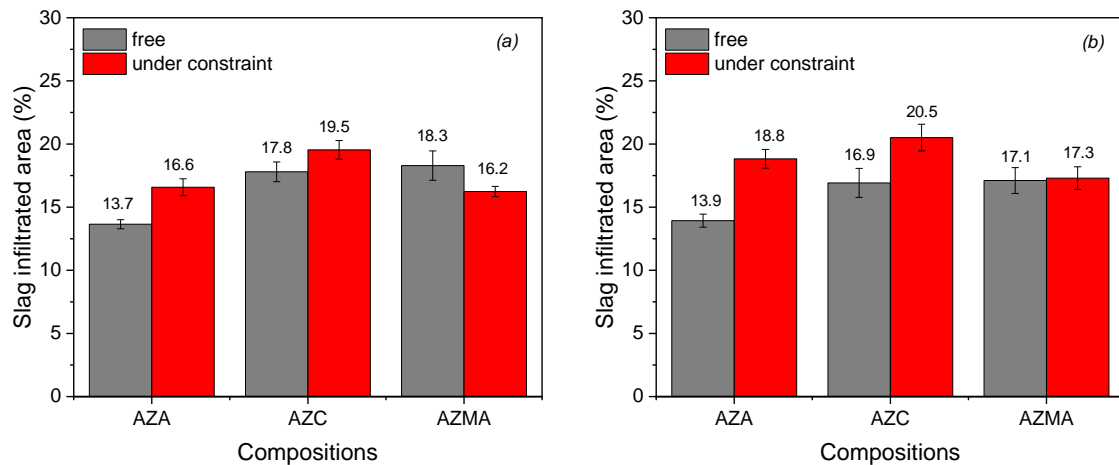

Figure 5 – Calculated slag infiltrated area when evaluating (a) calcined (600 °C for 5 h) or (b) fired (1500 °C for 5 h) castables, considering samples' free or under constraint. The corrosion cup tests were carried out at 1500 °C for 2 h.

When no restriction to the samples' expansion was imposed during the corrosion measurements (named here as "free", Fig. 5), AZA castable was the one that presented the best performance regardless of its previous thermal treatment (calcined or pre-fired), whereas AZMA showed the highest liquid infiltration, especially when the in situ spinel formation took place in the refractory microstructure during the corrosion test (Fig. 5a). Considering the generation of $MgAl_2O_4$ and $ZnAl_2O_4$ and their effects (i.e., significant changes in AZMA dimension during heating, as shown in Fig. 2), most likely the molten slag was able to find more available paths that favored its penetration in a greater extended manner in the castable structure. Moreover, $MgAl_2O_4$ formation could only be detected when firing the AZMA

matrix's samples above 1200 °C (Table 6), which indicates that not all MgO and Al_2O_3 might have had the chance to fully react during the tests of the calcined AZMA material, as the corrosion measurements were carried out at 1500 °C for 2 h. On the other hand, the pre-firing treatment enhanced the corrosion behavior of the AZC and AZMA free samples (Fig. 5b), resulting in a decrease in their slag infiltration area (changing from 17.8% to 16.9% and 18.3% to 17.1%, respectively), when comparing them to the ones calcined at 600°C for 5h.

Regarding the corrosion behavior of the castables when they were kept under constraint, AZC was the one that presented the worst performance for both evaluated conditions (calcined or pre-fired samples, Fig. 5a and 5b). Similar infiltrated area values were obtained for AZA and AZMA calcined refractories (16.6 % and 16.2 %, respectively) and the latter also showed an increase of the liquid penetration in the pre-fired specimens (17.3 %, Fig. 5b). Hence, the lack of freedom to expand affected in some extend the corrosion resistance of the evaluated castables. Some authors [37,38] highlight that refractories subjected to a geometrically constrained environment might present densification of their microstructures when exposed to high temperatures, which prevent further slag infiltration and corrosion during use, although these statements might change for other systems. Nevertheless, further investigations are still required to better analyze such aspects, as well as the distribution of the formed phases and the interaction of the slag-refractory at the interface of these materials.

Thermodynamic simulations were carried out to provide some insights on which phases should be formed during the slag-refractory contact at 1500 °C. Fig. 6 points out some diagrams where all likely proportions between the refractory composition and the slag were studied as a function of the reaction rate <A> at 1500 °C. The reaction rate <A> was defined by the ratio: (R)/[(S) + (R)] with (S) + (R) = 1 (R is the refractory and S the slag). More details of the simulation procedure can be found elsewhere [39].
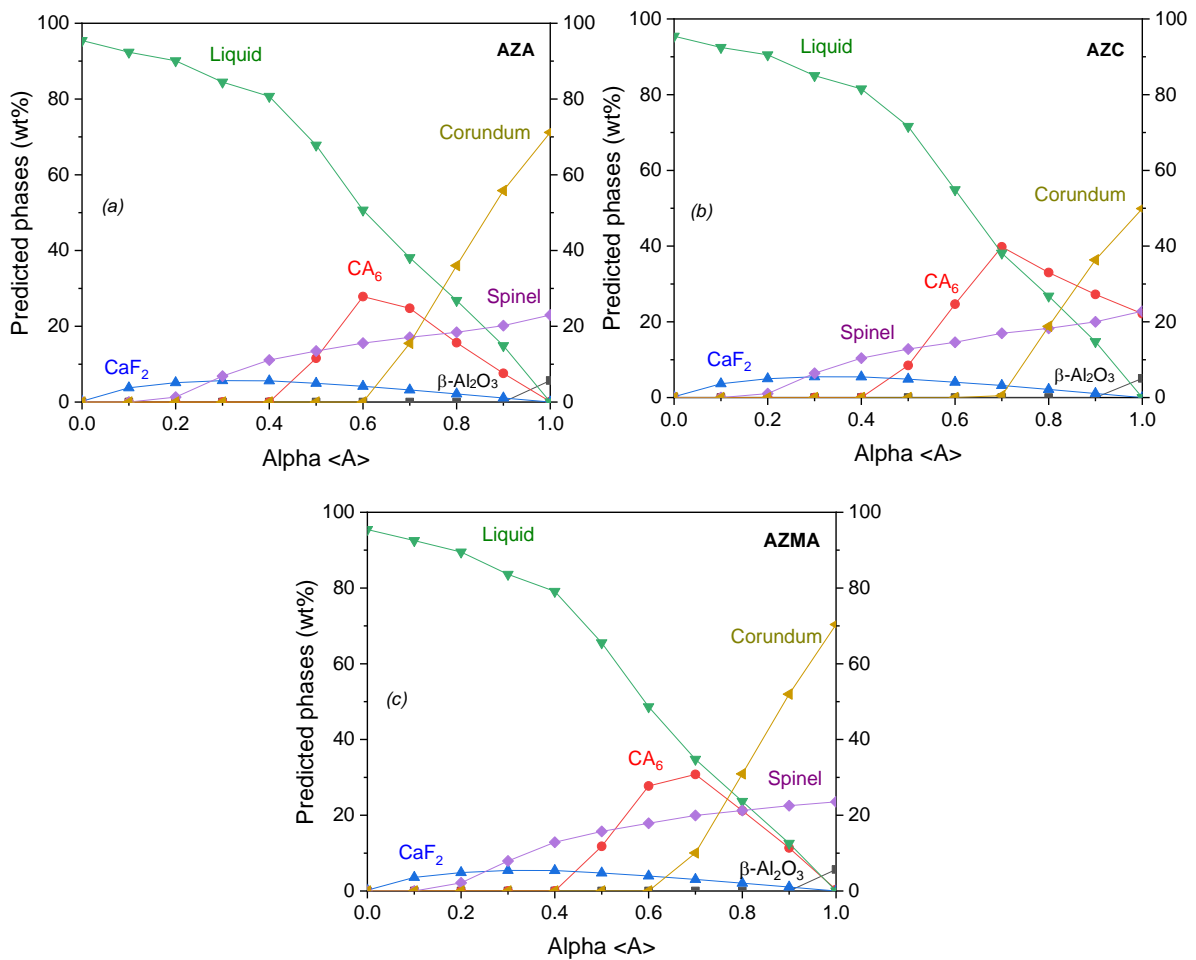
Figure 6 – Predicted phases obtained via thermodynamic calculations for the interaction between refractories (a) AZA, (b) AZC and (c) AZMA with a synthetic slag at 1500 °C and pressure = 1 atm.

In all graphs, the predicted overall refractory composition (comprising aggregates and fine raw materials) at 1500 °C is presented on the right Y axis of the figure (when <A> is equivalent to 1). According to Fig. 6, the ZnO-containing compositions should present corundum, spinel(ss) and beta-alumina in their microstructure at high temperature. Besides that, AZC also presents CA_6 (as previously pointed in the XRD results and the simulations regarding the matrix components, Tables 6 and 7, respectively) due to the use of calcium aluminate cement in such composition. After interacting with the molten slag, corundum is consumed by

reacting with CaO, derived from the liquid (Table 4), to give rise to $CaAl_{12}O_{19}$ (CA_6). Spinel ($ZnAl_2O_4$ and/or $MgAl_2O_4$) is the most resistance phase to the slag attack at 1500 °C, as it is not dissolved in the liquid formed with the selected slag and its presence was identified in all compositions even when changing the reaction rate <A> parameter.

Few changes in the content of phases could be identified when comparing the thermodynamic results predicted for the evaluated castables (Fig. 6), which indicates that from a chemical point of view, the compositions should present a similar corrosion behavior. However, other physical aspects are also important (i.e., samples' porosity, presence of cracks or flaws in the microstructure, etc.) as they influence the slag penetration rate and, consequently, the refractories' dissolution, as well as further precipitation of new phases, such as the predicted CA_6. The experimental corrosion measurements highlighted that the liquid infiltration area varied from 13.7 % to 20.5 % in the analyzed conditions, but further microstructural analyses of the corroded samples (mainly the slag-refractory interface) are still required to better understand the distribution and morphology of the phases contained in such materials. Such subjects should be explored in a forthcoming paper by the authors.

4. Conclusions

Based on the presented results, the following conclusions might be pointed out:

- Depending on the selected binder (hydratable alumina or calcium aluminate cement), distinct water content was required during the castables preparation to reach a suitable flowability level. Hence, such an aspect is important to be considered as not only distinct phases will be formed in the refractories' microstructure during their curing and heating treatments, but also the addition of

higher liquid content of AZA and AZMA increased their porosity and negatively affected the obtained mechanical strength values.

- The addition of high amount of ZnO or MgO (3 wt% to 9.4 wt%) to the castables resulted in the expansion of the samples during their first thermal treatment up to 1500 °C, reaching values of dL/L_0 equivalent to 1.16 %, 1.90 % and 2.35 % for AZA, AZMA and AZC, respectively. This behavior is associated with an expansive reaction that takes place during heating, due to the formation of $ZnAl_2O_4$, $MgAl_2O_4$, CA_2 and CA_6 in such materials. Based on the *in situ* elastic modulus and assisted sinterability tests, $ZnAl_2O_4$ was mainly formed above 800 °C, favoring an earlier sintering of the samples.

- No liquid phase formation was predicted to be found in the designed compositions up to 1500 °C, as well as no deformation of the samples was identified in the refractoriness under load tests, indicating that such materials present high thermal stability and are suitable for applications at high temperatures.

- Among the phases present in the ZnO-containing castables, spinel phase is an important one, as it presents higher chemical stability (based on the thermodynamic simulations) when in contact with the selected slag at high temperatures. Depending on the corrosion cup-test procedure (free or under constraint), different results of the slag infiltrated area were obtained (13.7 % to 20.5 %). AZA and AZC castables presented better corrosion resistance when they were free to expand during the measurements, regardless of the thermal treatment of the samples (calcined or pre-fired). On the other hand, AZMA (which contains $MgAl_2O_4$ and $ZnAl_2O_4$ phases in its structure) showed enhanced corrosion behavior when the tests were carried out under constraint. Further investigations are still required to better analyze the distribution of the formed phases and the interaction of the slag-refractory at the

interface of the designed castables and this should be explored in a forthcoming paper by the present authors.

5. Acknowledgments

6. References

[1]   S. Mukhopadhyay, P.K. Das Poddar, Effect of preformed and in situ spinels on microstructure and properties of a low cement refractory castable, Ceram. Int. 30 (2004) 369–380.

[2]   S. Zhang, W.E. Lee, Spinel-containing refractories, in: Refract. Handb., 2004: pp. 215–258.

[3]   T.M. Souza, A.P. Luz, C. Pagliosa, V.C. Pandolfelli, Mineralizing alumina-magnesia cement-bonded castables containing magnesium borates, Ceram. Int. (2015). https://doi.org/10.1016/j.ceramint.2015.05.063.

[4]   M. Fuhrer, A. Hey, W.E. Lee, Microstructural evolution in self-forming spinel-calcium aluminate castable refractories, J. Eur. Ceram. Soc. 18 (1998) 813–820.

[5]   D. Schmidtmeier, G. Buchel, A. Buhr, Magnesium aluminate spinel raw materials for high performance refractories for steel ladles, Ceram. Mater. 61 (2009) 223–227.

[6]   Y. Li, L. Guo, L. Chen, D. Ding, G. Ye, Effect of $Zn(OH)_2$ on properties of corundum based castables bonded with calcium aluminate cement, Ceram. Int. 47 (2021) 57–63.

[7]   M.A.L. Braulio, M. Rigaud, A. Buhr, C. Parr, V.C. Pandolfelli, Spinel-containing alumina-based refractory castables, Ceram. Int. 37 (2011) 1705–1724.

[8]   L. Guo, X. Wang, Y. Li, Y. Mu, Q. Jia, G. Wang, L. Chen, Evolution in properties of high alumina castables containing basic zinc carbonate, Ceram. Int. 47 (2021) 19019–19025.

[9]   A.P. Luz, M.A.L. Braulio, V.C. Pandolfelli, Spinel-containing alumina-based refractory castables, in: Refract. Castable Eng., Goller-Verlag, Baden-Baden, 2015: pp. 497–592.

[10]   A. Ghosh, S.K. Das, J.R. Biswas, H.S. Tripathi, G. Banerjee, The effect of ZnO addition on the densification and properties of magnesium aluminate spinel, Ceram. Int. 26 (2000) 605–608.

[11]   Z. Bi, R. Zhang, X. Wang, S. Gu, B. Shen, Y. Shi, Z. Liu, Y. Zheng, Synthesis of zinc aluminate spinel film through the solid-phase reaction between zinc oxide film and alpha-alumina substrate, J. Am. Ceram. Soc. 86 (2003) 2059–2062.

[12]   A.P. Luz, L.B. Consoni, C. Pagliosa, C.G. Aneziris, V.C. Pandolfelli, MgO fumes as a potential binder for in situ spinel containing refractory castables, Ceram. Int. (2018). https://doi.org/10.1016/j.ceramint.2018.05.201.

[13]   K. Goto, B.B. Argent, W.E. Lee, Corrosion of $MgO\text{-}MgAl_2O_4$ spinel refractory bricks by calcium aluminosilicate slag, J. Am. Ceram. Soc. 80 (1997) 461–471.

[14]   J.P. Guha, Reaction chemistry in dissolution of polycrystalline alumina in lime-alumina-

silica slag, Br. Ceram. Trans. J. 96 (1997) 231–236.

[15] J. Mori, M. Yoshimura, Y. Oguchi, T. Kawakami, Effect of slag composition on wear of alumina-spinel castable for steel ladle, Taikabutsu Overseas. 12 (1992) 40–45.

[16] A.G. Tomba Martinez, A.P. Luz, M.A.L. Braulio, E.Y. Sako, V.C. Pandolfelli, Revisiting CA_6 formation in cement-bonded alumina-spinel refractory castables, J. Eur. Ceram. Soc. (2017). https://doi.org/10.1016/j.jeurceramsoc.2017.07.003.

[17] E.Y. Sako, M.A.L. Braulio, A.P. Luz, E. Zinngrebe, V.C. Pandolfelli, Slag resistance of Al_2O_3-MgO refractory castables in different environmental conditions, J. Am. Ceram. Soc. 96 (2013) 3252–3257. https://doi.org/10.1111/jace.12433.

[18] P. Jeschke, G. Mortl, Recent tendencies in refractories for iron and steel production, in: Proc. UNITECR 1997, 1997: pp. 17–67.

[19] P. Xu, H. Wang, L. Ren, B. Tu, W. Wang, Z. Fu, Theoretical study on composition-dependent properties of $ZnO.nAl_2O_3$ spinels. Part II: Mechanical and thermophysical, J. Am. Ceram. Soc. (2021) jace.17997. https://doi.org/10.1111/jace.17997.

[20] P. Xu, H. Wang, L. Ren, B. Tu, W. Wang, Z. Fu, Theoretical study on composition-dependent properties of $ZnO.nAl_2O_3$ spinels. Part I: Optical and dielectric, J. Am. Ceram. Soc. (2021) jace.17756. https://doi.org/10.1111/jace.17756.

[21] D.L. Branson, Kinetics and mechanism of the reaction between zinc oxide and aluminum oxide, J. Am. Ceram. Soc. 48 (1965) 591–595.

[22] X.-J. Wang, Y.-M. Tian, J.-Y. Hao, Y.-Y. Wang, P.-B. Bai, Sintering mechanism and properties of $MgAl_2O_4$-$CaAl_{12}O_{19}$ composites with ZnO addition, J. Eur. Ceram. Soc. 40 (2020) 6149–6154.

[23] O.H. Borges, T. dos Santos Jr, V.R. Salvini, V.C. Pandolfelli, CA_6-based macroporous refractory thermal insulators containing mineralizing agents, J. Eur. Ceram. Soc. 40 (2020) 6141–6148. https://doi.org/10.1016/j.jeurceramsoc.2020.07.011.

[24] W.S. Hong, L.C. De Jonghe, X. Yang, M.N. Rahaman, Reaction sintering of ZnO-Al$_2$O$_3$, J. Am. Ceram. Soc. 78 (1995) 3217–3224.

[25] C. Leblud, M.R. Anseau, E. Di Rupo, F. Cambier, P. Fierens, Reaction sintering of ZnO-Al$_2$O$_3$ mixtures, J. Mater. Sci. 16 (1981) 539–544.

[26] Z. Nakagawa, Expansive behavior of powder compacts during spinel formation, Mass Charg. Transp. Ceram. (1996) 283–294.

[27] A. Nagasoe, S.I. Tsurumoto, A. Kitamura, Refractory characteristics of spinels with various MgO contents, Taikabutsu Overseas. 11 (1991) 20–28.

[28] D.R. Dinger, J.E. Funk, Particle packing, part II: Review of packing of polydisperse particle systems, InterCeram Int. Ceram. Rev. 41 (1992) 95–97.

[29] R.G. Pileggi, A.E. Paiva, J. Gallo, V.C. Pandolfelli, Novel rheometer for refractory castables, Am. Ceram. Soc. Bull. 79 (2000) 54–58.

[30] T.M. Souza, A.P. Luz, M.A.M. Brito, V.C. Pandolfelli, In situ elastic modulus evaluation of Al$_2$O$_3$-MgO refractory castables, Ceram. Int. 40 (2014) 1699–1707. https://doi.org/10.1016/j.ceramint.2013.07.066.

[31] M.A.L. Braulio, A.G.T. Martinez, A.P. Luz, C. Liebske, V.C. Pandolfelli, Basic slag attack of spinel-containing refractory castables, Ceram. Int. 37 (2011) 1935–1945. https://doi.org/10.1016/j.ceramint.2011.02.007.

[32] R.P. Racher, R. Kockegey, G. Buchel, A. Buhr, D. Gierisch, Improvement in workability behavior of calcia-free hydratable alumina binders, in: Proc. Unitecr 2005, Orlando, USA, 2005: pp. 402–407.

[33] W.E. Lee, W. Vieira, S. Zhang, K. Ghanbari-Ahari, H. Sarpoolaky, C. Parr, Castable refractory concretes, Int. Mater. Rev. 46 (2001) 145–167.

[34] C. Parr, J.M. Auvray, J. Pelletier, M. Szepizdyn, C. Wohrmeyer, C. Zetterström, A review of refractory bond systems for monolithic castable refractories, in: Proc. Fiftieth

Annu. Symp. Refract., Saint Louis, USA, 2014: pp. 18–35.

[35] M.A.L. Braulio, D.H. Milanez, E.Y. Sako, L.R.M. Bittencourt, V.C. Pandolfelli, Expansion behavior of cement bonded alumina-magnesia refractory castables, Am. Ceram. Soc. Bull. 86 (2007) 9201–9206.

[36] M.A.L. Braulio, P.O.R.C. Brant, L.R.M. Bittencourt, V.C. Pandolfelli, Microsilica or MgO grain size: Which one mostly affects the in situ spinel refractory castable expansion?, Ceram. Int. 35 (2009) 3321–3334.

[37] J. Soudier, P. Meunier, V. Nozahic, Characterisation of alumina-magnesia castables after firing in expansion controlled environment, in: Proc. Unitecr 2009, 2009: pp. 1–4.

[38] M.A.L. Braulio, E.Y. Sako, V.C. Pandolfelli, Expansion under constraint and its effect on high-alumina spinel-forming refractory castables, in: Proc. Unitecr 2013, 2013: pp. 708–713.

[39] J. Berjonneau, P. Prigent, J. Poirier, The development of a thermodynamic model for Al_2O_3-MgO refractory castable corrosion by secondary metallurgy steel ladle slags, Ceram. Int. 35 (2009) 623–635.